Two New 2p–3d Metal Complexes with a Nitronyl-Nitroxide Ligand Derived from o-Vanillin: Synthesis, Crystals Structures and Magnetic Properties

Cristian Andrei Spinu, Daniel O T A Martins, Teodora Mocanu, Mihaela Hillebrand, Jean-Pascal Sutter, Floriana Tuna, Marius Andruh

magnetochemistry

MDPI

Article

Two New 2p–3d Metal Complexes with a Nitronyl-Nitroxide Ligand Derived from *o*-Vanillin: Synthesis, Crystals Structures and Magnetic Properties

Cristian Andrei Spinu [1,2], Daniel O. T. A. Martins [3], Teodora Mocanu [4], Mihaela Hillebrand [5], Jean-Pascal Sutter [6,*], Floriana Tuna [3,*] and Marius Andruh [1,2,*]

[1] Inorganic Chemistry Laboratory, Faculty of Chemistry, University of Bucharest, Regina Elisabeta Blvd. 4-12, 030018 Bucharest, Romania; cristian.spinu@icoscdn.ro
[2] C. D. Nenitzescu Institute of Organic Chemistry and Supramolecular Chemistry of the Romanian Academy, Splaiul Independentei, 202B, 060023 Bucharest, Romania
[3] Department of Chemistry and Photon Science Institute, University of Manchester, Oxford Road, Manchester M13 9PL, UK; tavaresmartins.daniel@gmail.com
[4] "Ilie Murgulescu" Institute of Physical Chemistry, Romanian Academy, Splaiul Independenței 202, 060021 Bucharest, Romania; teo_mocanu_sl@yahoo.com
[5] Physical Chemistry Department, Faculty of Chemistry, University of Bucharest, 030018 Bucharest, Romania; mihaela.hillebrand@gmail.com
[6] Laboratoire de Chimie de Coordination du CNRS (LCC), Université de Toulouse, CNRS, 31077 Toulouse, France
* Correspondence: jean-pascal.sutter@lcc-toulouse.fr (J.-P.S.); floriana.tuna@manchester.ac.uk (F.T.); marius.andruh@acad.ro (M.A.)

Abstract: Two new 2p–3d complexes, $(Et_3NH)[ML(hfac)_2]$, have been obtained using the nitronyl-nitroxide radical (HL) derived from 2-hydroxy-3-methoxy-5-nitrobenzaldehyde (M = Mn **1**; Co **2**). The two compounds are isomorphous and their structures consist of anionic mononuclear species, $[M(hfac)_2L]^-$, M = Mn **1**; Co **2**, and triethylammonium cations, Et_3NH^+. The metal ions adopt an octahedral geometry, being coordinated by phenoxido and aminoxyl oxygen atoms from the ligand and four oxygen atoms from the hexafluoroacetylacetonato ($hfac^-$) ligand. The cryomagnetic behaviors of the two compounds reveal relatively strong antiferromagnetic M(II)-Rad interactions ($J_{MnRad} = -191$ cm^{-1}, $J_{CoRad} = -166$ cm^{-1} with $\boldsymbol{H} = -J\boldsymbol{S}_M\boldsymbol{S}_{Rad}$). The EPR spectra (X- and Q-band) of compound **1** below 70 K show the characteristical features of a $S = 2$ spin system with zero field splitting terms of $D = 0.26$ cm^{-1} and $E = 0.031$ cm^{-1}.

Keywords: manganese(II) complexes; cobalt(II) complexes; nitronyl-nitroxide ligands; EPR spectra; cryomagnetic measurements

Citation: Spinu, C.A.; Martins, D.O.T.A.; Mocanu, T.; Hillebrand, M.; Sutter, J.-P.; Tuna, F.; Andruh, M. Two New 2p–3d Metal Complexes with a Nitronyl-Nitroxide Ligand Derived from *o*-Vanillin: Synthesis, Crystals Structures and Magnetic Properties. *Magnetochemistry* **2024**, *10*, 86. https://doi.org/10.3390/magnetochemistry10110086

Academic Editors: Carlos J. Gómez García and Salah-Eddine Stiriba

Received: 1 October 2024
Revised: 25 October 2024
Accepted: 28 October 2024
Published: 1 November 2024

1. Introduction

Numerous molecular magnetic materials are obtained by combining organic radicals with either 3d or 4f metal ions [1–6]. Such paramagnetic ligands belong to different families: TEMPO, verdazyl, and nitronyl-nitroxide derivatives. The most popular radicals used as ligands are nitronyl-nitroxide (Nit) compounds, which generate a very rich coordination chemistry, consisting of discrete mono- and oligonuclear complexes up to coordination polymers (mainly 1D and 2D). We recall here that the first single chain magnet (SCM) [7], and SCMs with large coercive field [8,9] are 1D coordination polymers constructed from cobalt(II) ions and nitronyl-nitroxide ligands.

Let us briefly review the chemistry of manganese(II)-Nit molecular magnetic materials. The coordinating abilities of the Nit ligands can be tuned by ligand functionalization. A plethora of manganese(II) complexes have been synthesized with such ligands, varying from mononuclear [10–16] and oligonuclear species [10,17–25], to 1D coordination polymers [26,27]. Mononuclear complexes have been obtained by reacting 2-pyridyl [11,14],

triphenylphosphine oxide [10], amide [12,13], and triazole [15,16] substituted nitronyl-nitroxide ligands, with manganese(II) chloride, perchlorate and, most frequently, hexafluoroacetylacetonate. With longer ligands displaying coordination sites well separated from one another, such as 4-pyridyl [17], 4-quinolyl [18], 4-(5-pyrimidyl)phenyl [19], 4-(1-imidazole)phenyl [20], 2-quinoxalinyl [21], 4-(carboxyl)phenyl [22], 3-(*m*-pyridyl)-2-thienyl [23], 4-(3-pyridinylmethoxy)phenyl [24], and 3-((1*H*-1,2,4-triazol-1-yl)methoxy)-phenyl [25], the resulted complexes are binuclear. A smaller ligand, 3-isobutyl-pyrazole substituted nitronyl-nitroxide, generates a 1D-chain [27]. 2D coordination polymers have been obtained from nitronyl-nitroxide ligands decorated with imidazole and benzimidazole fragments by using a molar ratio metal:ligand of 2:3. [28–30]. Low nuclearity manganese(II)-(nitronyl-nitroxide) complexes, particularly mononuclear ones, are useful models for magneto-structural correlations.

In this paper we report on the crystal structures and magnetic properties of two 3D metal complexes containing a nitronyl-nitroxide ligand, $(Et_3NH)[M(hfac)_2L]$, where M = Mn(II) **1**, Co(II) **2**, and HL = 2-(2-hydroxy-3-methoxy-5-nitrophenyl)-4,4,5,5-tetramethyl-4,5-dihydro-1H-imidazol-3-oxide-1-oxyl (Scheme 1).

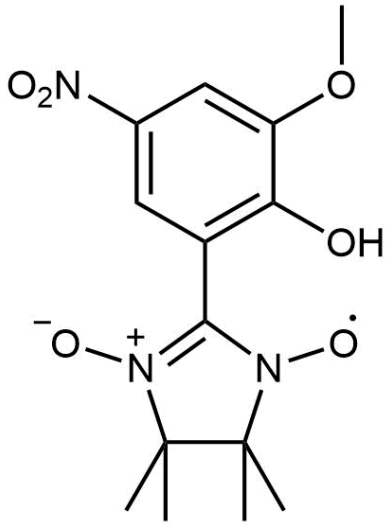

Scheme 1. Structure of HL ligand.

2. Experimental Part

2.1. Materials and Methods

The 2-(2-Hydroxy-3-methoxy-5-nitrophenyl)-4,4,5,5-tetramethyl-4,5-dihydro-1H-imidazol-3-oxide-1-oxyl (HL) ligand was synthesized as previously described [31]. All other reagents and solvents were commercially purchased and used without any further purification, if not stated otherwise. Elemental analyses (C, H, N) were performed on a EuroEA Elemental Analyzer.

2.2. Synthesis of the Complexes

2.2.1. Synthesis of $(Et_3NH)[MnL(hfac)_2]$ **1**

$Mn(hfac)_2{\cdot}2H_2O$ (0.073 g, 0.1443 mmol) was dissolved in 10 mL of heptane and refluxed for 30 min. Then, after cooling down the solution, another 10 mL of CH_2Cl_2 solution containing HL (0.047 g, 0.1443 mmol) and triethylamine (0.0146 g, 0.1443 mmol, 20 µL) was added over. The solution was refluxed for 30 min, cooled down and filtered. After allowing the solvent to slowly evaporate for three days, violet needle shaped crystals of the product were obtained 0.070 g, yield 54%. Anal. Calcd for $C_{30}H_{35}O_{10}N_4F_{12}Mn$ (%): C, 40.28; H, 3.94; N, 6.26; Found: C, 40.01; H, 3.11; N, 5.91. Selected IR peaks (cm^{-1}): 3420 (w), 2992 (w), 2957 (w), 2837 (w), 2691 (w), 1649 (s), 1599 (w), 1555 (m), 1528 (m), 1503 (vs), 1455 (m), 1398 (w), 1366 (m), 1329 (s), 1308 (s), 1254 (vs), 1202 (s), 1144 (vs), 1103 (m), 1071 (w),

978 (w), 947 (w), 870 (w), 831 (w), 797 (w), 764 (w), 743 (w), 665 (m), 583 (w), 544 (w), 529 (w), 451 (w). UV-Vis (nm): 428, 547, 589.

2.2.2. Synthesis of $(Et_3NH)[CoL(hfac)_2]$ **2**

$Co(hfac)_2 \cdot 2H_2O$ (0.073 g, 0.1443 mmol) was dissolved in 10 mL of heptane and refluxed for 30 min. Then, after cooling down the solution, another 10 mL of CH_2Cl_2 solution containing HL (0.047 g, 0.1443 mmol) and triethylamine (0.0146 g, 0.1443 mmol, 20 µL) was added over. The solution was refluxed another 30 min, cooled down and filtered. After allowing the solvent to slowly evaporate for three days, violet needle shaped crystals of the product were obtained 0.085 g, yield 65%. Anal. Calcd for $C_{30}H_{35}O_{10}N_4F_{12}Co$ (%): C, 40.10; H, 3.93; N, 6.24; Found: C, 39.99; H, 3.84; N, 5.62. Selected IR peaks (cm^{-1}): 3092 (w), 2991 (w), 2951 (w), 2839 (w), 2685 (w), 1643 (s), 1601 (w), 1555 (m), 1526 (m), 1504 (s), 1452 (m), 1396 (w), 1364 (m), 1329 (m), 1310 (s), 1256 (vs), 1204 (vs), 1146 (vs), 1094 (m), 1070 (w), 980 (w), 947 (w), 870 (w), 849 (w), 795 (m), 764 (w), 744 (w), 671 (m), 584 (w), 544 (w), 528 (w), 451 (w). UV-Vis (nm): 426, 538, 610, 1230.

3. Physical Measurements

IR spectra were recorded on a FTIR Bruker Tensor V-37 spectrophotometer (KBr pellets) in the range of 4000–400 cm^{-1} (Figure S1). UV-Vis diffuse reflectance spectra were recorded on a JASCO V-670 spectrophotometer on undiluted samples in the range 200–1600 nm. The X-Ray powder diffraction measurements (XRPD) were carried out on a Proto AXRD Benchtop using the Cu-Kα radiation with a wavelength of 1.54059 Å in the range 5–35° 2θ.

Continuous-wave (CW) electron paramagnetic resonance (EPR) spectra were recorded on a Bruker EMX 300 EPR spectrometer operating at X- (~9.4 GHz) or Q-band (~34 GHz) microwave frequencies, and at variable temperatures in the range 5 to 298 K. Spectra were simulated using the EasySpin 6.0.6 software [32].

Magnetic measurements were carried out with a Quantum Design MPMS 5S SQUID magnetometer in the temperature range 2−300 K. The measurements were performed on crystalline powders of the complexes mixed with grease (for Co) and hold in a gelatin capsule. The temperature dependences of the magnetization were measured in an applied field of 1 kOe and the isothermal field dependence of the magnetizations were collected up to 50 kOe. The molar susceptibility (χ_M) was systematically corrected for sample holder, grease and for the diamagnetic contribution of all the atoms by using Pascal's tables [33]. AC susceptibility has been collected in zero field and with applied field with an AC frequency of 1000 Hz.

4. Crystal Structure Determination and Refinement

Suitable single crystals were mounted on glass fiber and X-Ray data were collected on a Rigaku XtaLAB Synergy, Single source at offset/far, HyPix (**1**) and STOE IPDS II (**2**) diffractometers using a graphite-monochromated Mo Kα radiation source (λ = 0.71073Å). The structures were solved by direct methods and refined by full-matrix least squares techniques based on F^2 using SHELXTL-2018 crystallographic software packages [34,35]. The non-H atoms were refined anisotropically. The H atoms attached to the C atoms were placed on calculated positions (riding model), while the H atoms on the N atoms of the triethylammonium cations were assigned using the residual peaks, and refined with isotropic thermal displacement parameters. The restraining DFIX and DANG commands were applied to rationalize the bond and angles parameters. A summary of the crystallographic data and the structure refinement for crystals **1** and **2** are given in Table 1. Selected bond distances and angle values are listed in Table 2. CCDC Reference numbers: 2,388,242 (**1**), 2,388,243 (**2**).

Table 1. Crystallographic data and structure refinement parameters for compounds **1** and **2**.

Compound	1-Mn	2-Co
Formula	$C_{30}H_{35}N_4O_{10}F_{12}Mn$	$C_{30}H_{35}N_4O_{10}F_{12}Co$
Formula weight	894.56	898.55
Crystal system	monoclinic	monoclinic
Space group	$P2_1/c$	$P2_1/c$
a/Å	20.4684(18)	20.150(3)
b/Å	9.5569(5)	9.5624(8)
c/Å	21.6281(17)	21.501(3)
β/°	111.421(9)	110.433(11)
V/Å^3	3928.5(6)	3882.0(9)
Z	4	4
D_c/g cm^{-3}	1.509	1.537
T/K	293(2)	293(2)
μ/mm^{-1}	0.448	0.556
Reflections collected	28,318	39,975
Independent reflection	6943 [R_{int} = 0.0487]	6840 [R_{int} = 0.1921]
Final R indices [$I > 2\sigma(I)$]	0.0478; 0.1247	0.0773; 0.1353
R indices (all data)	0.0772; 0.1404	0.1835; 0.1837
Goodness-of-fit on F^2	1.031	1.088
$\Delta\rho_{min}/\Delta\rho_{max}$ (e Å^{-3})	−0.27/0.52	−0.32/0.37

Table 2. Selected bond distances and angle values in compounds **1** and **2**.

1	2
Bonds length (Å)	
Mn1–O1 = 2.191(2)	Co1–O1 = 2.097(4)
Mn1–O3 = 2.121(2)	Co1–O3 = 2.033(5)
Mn1–O7 = 2.172(2)	Co1–O7 = 2.080(5)
Mn1–O8 = 2.162(2)	Co1–O8 = 2.040(5)
Mn1–O9 = 2.129(2)	Co1–O9 = 2.036(5)
Mn1–O10 = 2.162(2)	Co1–O10 = 2.073(5)
Angles (°)	
O1 Mn1 O3 = 84.6(2)	O1 Co1 O3 = 88.8(3)
O1 Mn1 O7 = 90.9(2)	O1 Co1 O7 = 90.3(2)
O1 Mn1 O8 = 171.3(2)	O1 Co1 O8 = 172.6(2)
O1 Mn1 O9 = 81.1(2)	O1 Co1 O9 = 81.2(2)
O1 Mn1 O10 = 98.5(2)	O1 Co1 O10 = 96.4(2)
O3 Mn1 O7 = 94.42(1)	O3 Co1 O7 = 92.3(2)
O3 Mn1 O8 = 100.6(1)	O3 Co1 O8 = 98.1(2)
O3 Mn1 O9 = 163.2(1)	O3 Co1 O9 = 169.0(2)
O3 Mn1 O10 = 89.4(1)	O3 Co1 O10 = 87.5(2)
O7 Mn1 O8 = 81.8(2)	O7 Co1 O8 = 87.1(2)
O7 Mn1 O9 = 94.7(1)	O7 Co1 O9 = 92.4(2)
O7 Mn1 O10 = 169.9(2)	O7 Co1 O10 = 173.2(3)
O8 Mn1 O9 = 94.5(1)	O8 Co1 O9 = 91.9(2)
O8 Mn1 O10 = 88.3(1)	O8 Co1 O10 = 86.2(2)
O9 Mn1 O10 = 83.8(1)	O9 Co1 O10 = 88.9(2)

5. Results and Discussion

The Nit ligand, HL, has been synthesized following Ullman's protocol starting from 2-hydroxy-3-methoxy-5-nitrobenzaldehyde (*o*-vanillin with the 5 position previously protected with a nitro group) [31]. We have tested the ability of HL molecules to form complexes by reacting it with M(hfac)$_2$, M = Ni(II), Zn(II), in the presence of Et_3N, to deprotonate the phenolic group [31]. The manganese and cobalt complexes, (Et_3NH)[Mn(hfac)$_2$L] **1**, (Et_3NH)[Co(hfac)$_2$L] **2**, are isomorphous with the nickel and zinc derivatives men-

tioned above. Therefore, we describe briefly the crystal structure of the manganese derivative. Compound $(Et_3NH)[Mn(hfac)_2L]$ **1** consists of an anionic mononuclear species, $[Mn(hfac)_2L]^-$ (Figure 1), and triethylammonium cations, Et_3NH^+. The metal ion adopts an octahedral coordination sphere, coordinated by phenoxido and aminoxyl oxygen atoms from the ligand and four oxygen atoms from the hexafluoroacetylacetonato ($hfac^-$) ligand. The Mn(II)–O bonds vary from 2.121(2) to 2.191(2) Å. The N1–O1 bond length from the coordinated aminoxyl group is 1.292(3) Å, slightly longer than the uncoordinated N2–O2 group (1.274(3) Å).

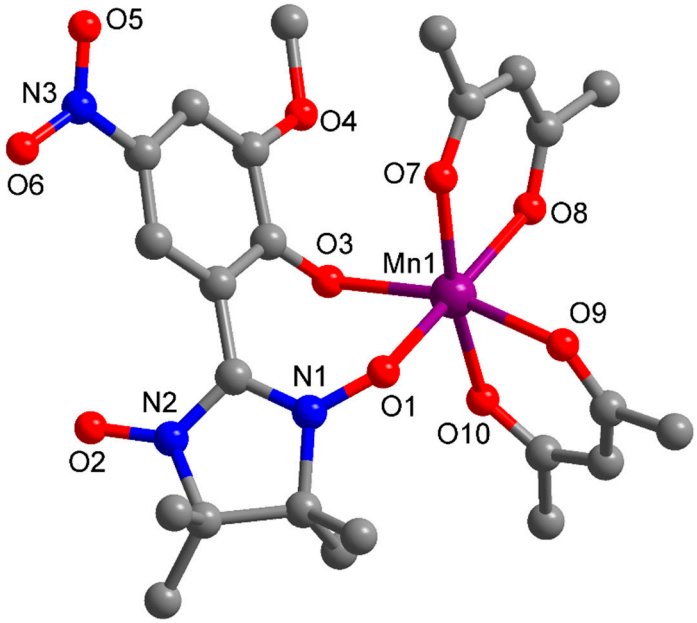

Figure 1. The X-ray structure of the complex anion in **1**; the hydrogen and fluorine atoms have been omitted for clarity.

In compound **1** the CF_3 groups are disordered over two crystallographic positions assigned as A (0.43) and B (0.57). For both crystallographic models, the packing diagram reveals a network of intermolecular F···F interactions (2.548–3.087 Å) connecting the mononuclear units at supramolecular level (Figures S2 and S3). The crystal structure of compound **2** is represented in Figure S4. The purity of the crystalline compounds, **1** and **2**, has been proved by powder X-Ray diffraction: the experimental diffractograms correspond well to the simulated ones (Figures S5 and S6).

The diffuse reflectance UV-Vis spectra of the ligand and the two complexes are displayed in Figure S7. Compound **2** shows, apart from the bands arising from the organic ligands, one d-d band at $^4T_1 \rightarrow {}^4T_2$ (1230 nm), assuming the *O* point group [36].

5.1. Magnetic Properties of **1** *and* **2**

Complexes **1** and **2** were studied by magnetometry, results are plotted as $\chi_M T$ = f(T) (where χ_M stands for the molar magnetic susceptibility) and M = f(H) in Figure 2 and Figure 4, respectively. The $\chi_M T$ product for **1** at 300 K is 3.27 $cm^3\ mol^{-1}$ K, which is smaller than the expected value of 4.75 $cm^3 mol^{-1}$K for uncoupled S = 5/2 (Mn^{II}) and S = 1/2 (radical) spins, suggesting significant antiferromagnetic coupling between Mn(II) and the paramagnetic ligand. The $\chi_M T$ value decreases as the temperature is reduced reaching a plateau below 150 K at about 3.1 $cm^3\ mol^{-1}$ K, and drops to a lower value below 50 K (Figure 2). The recorded $\chi_M T$ plateau corresponds to a S = 2 spin ground state resulted from the antiferromagnetic Mn^{II}—radical coupling. The data have been analyzed considering a S = 5/2 and a S = 1/2 in exchange interaction (J), possible weak inter-molecular interactions have been considered within the mean-field approximation (zJ'). Modeling was done using the PHI program [37]. The best fit to the data gives the following values (with respect to $\boldsymbol{H}$ =

$-JS_{Mn}S_{Rad}$): $J = -191$ cm^{-1}; $g_{Mn} = 2.032$; $g_{Rad} = 2.0$ (fixed), with very weak intermolecular interactions, $zJ' = -0.019$ cm^{-1}. The magnetization vs. field curve obtained at 2 K, reaches saturation to high field with a value of 3.92 μ_B, a slightly lower than the value anticipated for an $S = 2$ ground state.

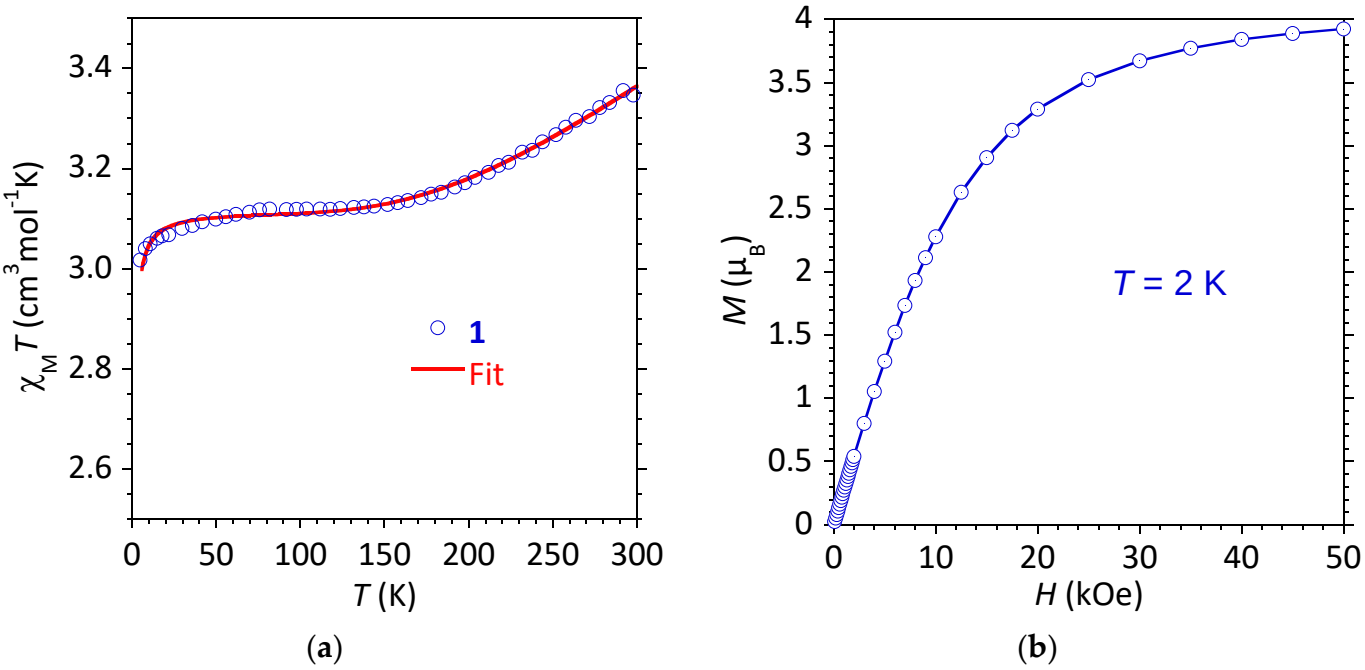

Figure 2. (**a**) Experimental (○) and calculated (—) temperature dependence of $\chi_M T$ and (**b**) field dependence of the magnetization at 2 K for compound **1**.

In the literature, the Mn(II)-Nit coupling is antiferromagnetic, with the exchange parameter J ranging from -0.74 to -213 cm^{-1} [10–16], which is strongly influenced by the values of the Mn–O–N and Mn–O–N–C (dihedral) angles, as well as the Mn–O(Nit) distance. Mn–O–N angles of ca. 125° lead to quite strong antiferromagnetic coupling between manganese (II) and the radical. Representative examples are presented in Table 3.

Table 3. Geometrical parameters and J values (with respect to $\boldsymbol{H} = -JS_{Mn}S_{Rad}$) for selected mononuclearMn(II)-Nit complexes.

Compound	$J_{Mn\text{-}NIT}$ (cm^{-1})	Mn–O (Å)	Mn–O–N (°)	Mn–O–N–C (°)	Ref.
[Mn(hfac)$_2$(*o*PONit)] [a]	−213	2.150(4)	124.7	83.1	[10]
[Mn(hfac)$_2$L^1] [b]	−114.4	2.181(2)	124.5	28.7	[12]
[Mn(NIT2Py)(NTB)](ClO$_4$)$_2$ [c]	−0.74	2.133(3)	132.9	20.4	[14]
[Mn(hfac)$_2$L^3] [d]	−193.4	2.129(3)	123.6	47.8	[15]
[Mn(hfac)$_2$(4-Me-3-Nit-trz)] [e]	−99.2	2.158(2)	117.2	51.9	[16]
(Et$_3$NH)[MnL(hfac)$_2$] **1**	−191	2.191(2)	128.1	57.9	this work

[a] *o*PONit = (o-nitronyl nitroxide-phenyl)diphenylphosphine oxide. [b] L^1 = 4,4,5,5-tetramethyl-4,5-dihydro-1H-imidazole-3-oxide-1-oxyl-2-carboxylic acid amide. [c] NIT2Py = 2-(2′-pyridyl)-4,4,5,5-tetramethylimidazoline-1-oxyl-3-oxide. [d] L^3 = 4,4,5,5-tetramethyl-2-(2-phenyl-1,2,3-triazole-4-yl)imidazoline-1–oxyl-3-oxide. [e] 4-Me-3-Nit-trz = 2-[3-(4-methyl-1,2,4-triazolyl)]-4,4,5,5-tetramethylimidazoline-1-oxyl-3-oxide.

The strong antiferromagnetic Mn(II)–Rad interaction is confirmed by DFT calculations, which were performed using the Gaussian09 program [38], maintaining the crystal geometry without optimization. Starting with the spins of the Mn(II) ion and of the radical, 5/2 and 1/2 respectively, two states were considered: a high spin (HS), $S = 3$, $2S + 1 = 7$ and a low spin (LS), in which the radical spin is antiparallel to that of the Mn ion, $S = 2$, $2S + 1 = 5$. The energy of the low spin state, hereafter labeled as the Broken Symmetry (BS) state, was calculated by the fragment procedure as implemented in the Gaussian09 program and further checked for its stability. Two functionals, uB3LYP [39] and uM06 [40] were used with the TZVP basis set [41]. The exchange coupling constant, J, was calculated using the literature Equations (1)–(3) [42,43]:

$$J = (E_{BS} - E_{HS})/(2S_{Mn}S_{Rad} + S_{Rad}) \quad (1)$$

$$J = 2(E_{BS} - E_{HS})/S^2_{max}\ (S_{max} = S_1 + S_2) \quad (2)$$

$$J = 2(E_{BS} - E_{HS})/(<S^2>_{HS} - <S^2>_{BS}) \quad (3)$$

The results presented in Table 4 reflect the antiferromagnetic behavior of the complex, the broken spin state (BS) being the ground state; as far as the J value is concerned, Equation (2) led to the closest agreement with the experimental value, $J_{exp} = -191$ cm^{-1}. It can also be remarked that both functionals lead to quite similar results.

Table 4. Energies of the low (BS) and high spin (HS) states and J values calculated using Equations (1)–(3).

Functional	E_{BS} (Ha)	E_{HS} (Ha)	J (cm^{-1})		
			(Equation (1))	(Equation (2))	(Equation (3))
uB3Lyp	−4192.3621525	−4192.3581071	−295.95	**−197.30**	−297.90
uM06	−4190.8464697	−4190.8426809	−277.18	**−184.79**	−279.09

The spin isodensity surfaces corresponding to the two spin states are displayed in Figure 3a (BS-state) and Figure 3b (HS-state). For both states the spin density is mainly localized on the Mn ion and to a lower extent on the nitronyl groups.

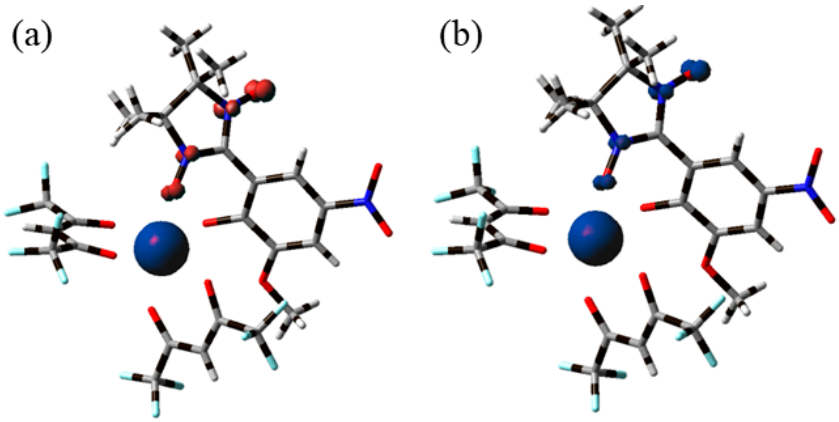

Figure 3. The spin density surfaces (isodensity = 0.04) for the BS (**a**) and HS (**b**) spin states at the uB3LYP/TZVP level.

The magnetic data of compound **2**, in the form of $\chi_M T$ vs. T and M vs. H/T, are shown in Figure 4. Due to the significant orbital contribution in octahedral geometry, the Co(II) ion is characterized by a $\chi_M T$ value that overcome the calculated spin-only value of 1.875 cm^3 mol^{-1} K and usually approaches 3 cm^3 mol^{-1} at 298 K [33,44,45]. Therefore, in the absence

of any interaction between Co and ligand, an approximate $\chi_M T$ value of 3.375 cm^3 mol^{-1} K would be expected for compound **2**. However, the measured $\chi_M T$ for **2** is 2.26 cm^3 mol^{-1} K at room temperature, and it decreases as the temperature is lowered. This suggests that strong antiferromagnetic coupling occurs between the Co(II) and the radical. The $\chi_M T(T)$ curve shows a steady decrease below 300 K, then an inflection is noticed around 130 K. Below this temperature, a faster decrease occurs, because of the thermal depopulation of the excited Kramers doublets of the Co(II) ions. Fitting of the data has assumed contributions from J_{CoRad}, D for Co(II), and possible intermolecular interactions considered within a mean field approximation (zJ'). The analysis was performed simultaneously on $\chi_M T$ and M = f(H/T). The following values have been obtained: g_{Co} = 2.417, $J = -166$ cm^{-1}, D = 65 cm^{-1}. The antiferromagnetic Co(II)-Rad interaction is quite strong (formalism: $\boldsymbol{H} = -J\boldsymbol{S}_{Co}\boldsymbol{S}_{Rad}$). However, some uncertainty applies because g_{Co} is not known precisely (that for the radical was fixed to 2 for the calculations). The field dependence of the magnetization is also well reproduced, as it is plotted in the form of M = f(H/T) in Figure 4b.

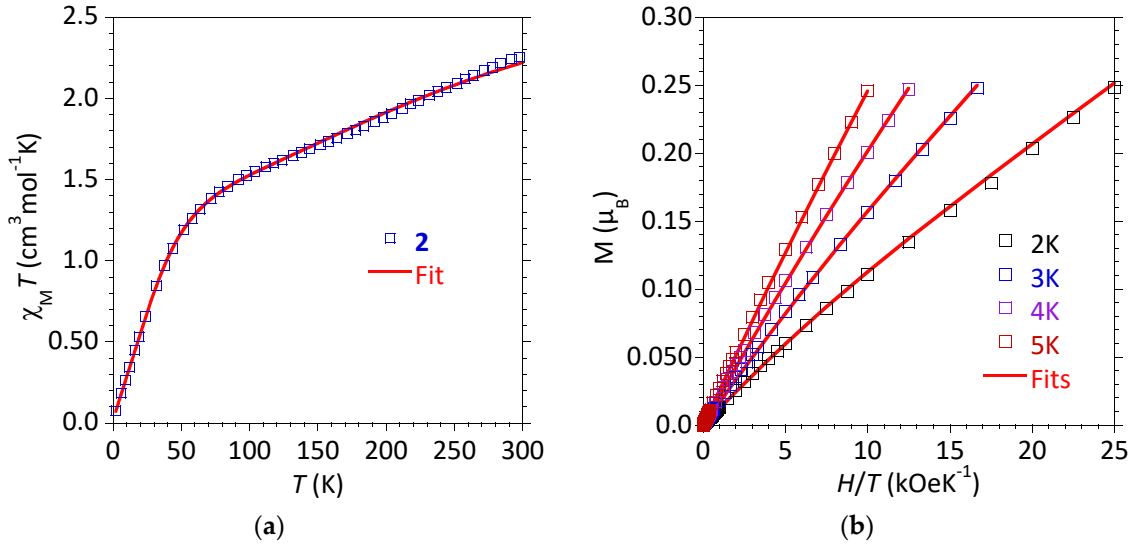

Figure 4. Experimental (□) and best fits (full red lines) for (**a**) $\chi_M T$ = f(T) and (**b**) M = f(H/T) behaviors for compound **2**.

If the magnetic data are represented as χ_M vs. T plot (Figure S8), after a plateau observed at 30 K, a Curie tail (i.e., an increase of the magnetic susceptibility) is clearly observed for lower T indicating the presence of a paramagnetic impurity. This χ_M vs. T curve was perfectly reproduced when a fraction (0.01) of a $S = 3/2$ impurity was considered. The contribution of this 0.01 fraction of S = 3/2 was taken into account for the analyses of $\chi_M T$ and M = f(H) discussed above.

AC magnetic susceptibility measurements between 2 and 15 K did not reveal any evidence for slow relaxation of the magnetization for this compound.

5.2. Electron Paramagnetic Resonance (EPR) Data for **1**

Continuous-wave (CW) EPR spectra for powder samples of **1** were recorded at X- (ca. 9.4 GHz) and Q-band (ca. 34 GHz) and several temperatures (Figures 5 and 6 respectively). Spectra recorded below 70 K show the clear characteristics of a $S = 2$ spin state that was stabilized by antiferromagnetic coupling between the spins of Mn(II) and Nit radical (see above). Here the zero-field splitting (ZFS) interaction $D[S_z^2 - (1/3)S(S+1)] - E(S_x^2 - S_y^2)$ splits the levels of an $S = 2$ spin state into two non-Kramer doublets, $|\pm 2\rangle$ and $|\pm 1\rangle$, and a singlet corresponding to the $m_S = 0$ [46]. Under the application of a magnetic field EPR transitions can occur within and between these splitting components leading to a multi-line

structure as observed in Figures 5 and 6. Simulation of the Q-band EPR spectrum at 9 K (Figure 7) using EasySpin [32], and the spin Hamiltonian (4):

$$\mathcal{H} = gBS_B + D\left[S_z{}^2 - (1/3)S(S+1)\right] + E\left(S_x{}^2 - S_y{}^2\right) \quad (4)$$

with $S = 2$, and D and E as the axial and rhombic zero-field splitting terms, respectively, provided $D = 0.26$ cm^{-1} and $E = 0.031$ cm^{-1}. ZFS is present in systems which $S > 1/2$ and is a result from both SOC and spin-spin coupling (SSC) interactions, the former being more prominent in transition metals. Although perfectly symmetric half-occupied *d*-orbitals should not present any SOC, some may arise if the compound deviates from a perfect symmetry [47].

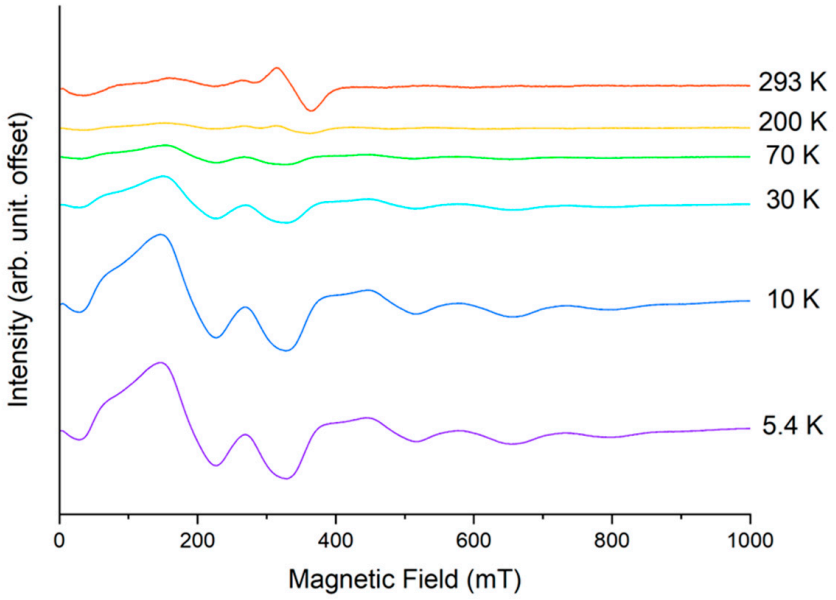

Figure 5. X-band (9.4 GHz) CW-EPR spectra of powder samples of **1** at temperatures between 5.4 and 293 K.

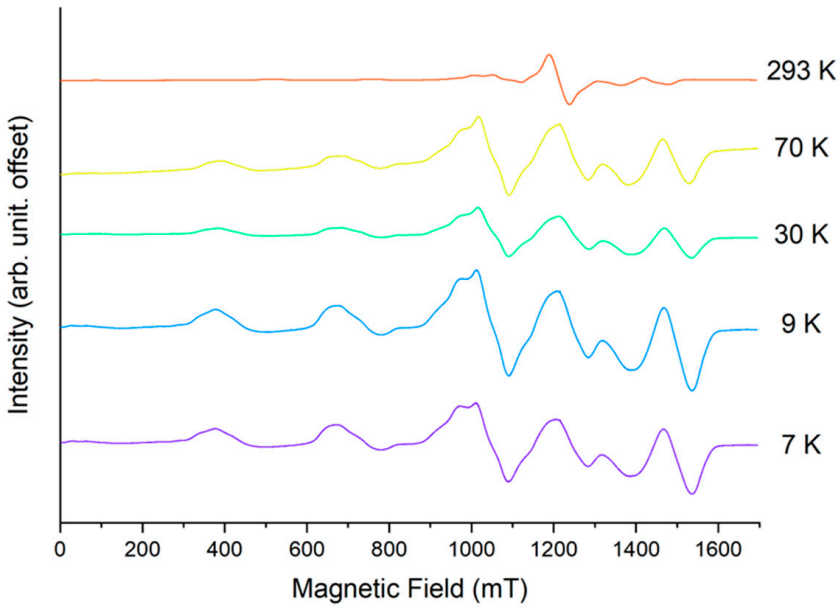

Figure 6. Q-band (34 GHz) CW-EPR spectra of powdered **1** at temperatures between 7 and 293 K.

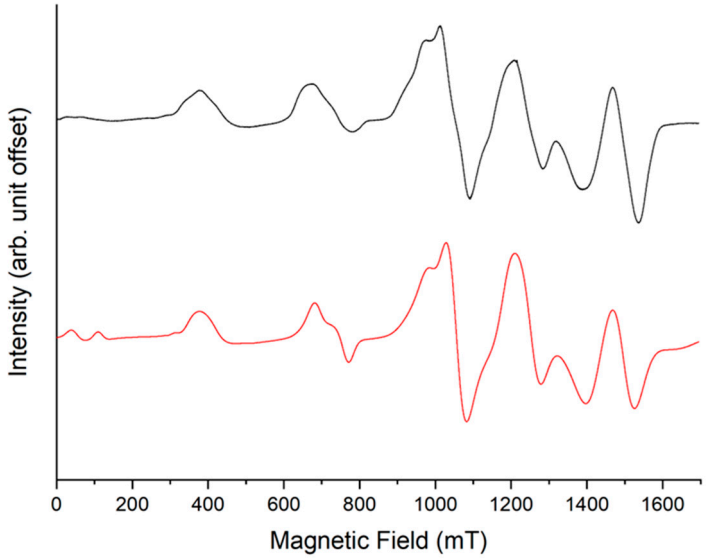

Figure 7. Experimental (black) and simulated (red) Q-band (34 GHz) CW-EPR spectra of powdered compound **1** at 9 K (g = 2, D = 0.26 cm^{-1}, E = 0.031 cm^{-1}, and H-Strain (x, y, z) = 1300, 2100, 2000 MHz).

6. Conclusions

Two 2p–3d mononuclear complexes have been synthesized and structurally characterized. For both Mn(II) and Co(II) compounds strong antiferromagnetic metal-radical interaction was found, with a significant Zero Field Splitting effect (D). The EPR investigation of the manganese derivative reveals the signature of an S = 2 ground state, in agreement with the magnetic measurements.

Supplementary Materials: The following supporting information can be downloaded at: https://www.mdpi.com/article/10.3390/magnetochemistry10110086/s1, Figure S1. Infrared spectra for HL and complexes **1** and **2**; Figure S2. The packing diagram of crystal **1** with the representation of F···F interactions taking into account the disorder of CF_3 group in position assigned A (0.43 occupancy); Figure S3. The packing diagram of crystal **1** with the representation of F···F interactions taking into account the disorder of CF_3 group in position assigned B (0.57 occupancy); Figure S4. The X-ray structure of the complex anion in **2**; the hydrogen and fluorine atoms have been omitted for clarity; Figure S5. Measured (red) and calculated (black) powder X-ray diffraction patterns of **1**; Figure S6. Measured (red) and calculated (black) powder X-ray diffraction patterns of **2**; Figure S7. Diffuse reflectance spectra for HL and complexes **1** and **2**; Figure S8. Experimental (□) and calculated (—) χ_M = f(T) for compound **2.** The best fit parameters are discussed in the main text.

Author Contributions: The manuscript was prepared with the contributions of all authors. They specifically contributed as follows: C.A.S.—Investigation; D.O.T.A.M.—Investigation. T.M.—Data curation; M.H.—Investigation; J.-P.S.—Investigation, Formal analysis; F.T.—Formal analysis; M.A., F.T. and J.-P.S.—Writing original draft, supervision. All authors have read and agreed to the published version of the manuscript.

Funding: This research was funded by UEFISCDI (Project PN-III-P4-ID-PCE-2016-0308I) and EPSRC UK (grants EP/W014521/1, EP/V035231/1 and EP/X034523/1).

Institutional Review Board Statement: Not applicable.

Informed Consent Statement: Not applicable.

Data Availability Statement: The original contributions presented in the study are included in the article and Supplementary Materials, further inquiries can be directed to the corresponding authors.

Acknowledgments: Authors are grateful to M. J.-F. Menier (LCC, Toulouse) for technical assistance in magnetic data collections and M. Răducă (ICOS, Bucharest) for X-ray powder diffraction data

collections. We further acknowledge the UK National EPR Facility at the University of Manchester for EPR data collection.

Conflicts of Interest: The authors declare no conflict of interest.

References

1. Vaz, M.G.F.; Andruh, M. Molecule-based magnetic materials constructed from paramagnetic organic ligands and two different metal ions. *Coord. Chem. Rev.* **2021**, *427*, 213611. [CrossRef]
2. Meng, X.; Shi, W.; Cheng, P. Magnetism in one-dimensional metal–nitronyl nitroxide radical system. *Coord. Chem. Rev.* **2019**, *378*, 134–150. [CrossRef]
3. Demir, S.; Jeon, I.-R.; Long, J.R.; Harris, T.D. Radical ligand-containing single-molecule magnets. *Coord. Chem. Rev.* **2015**, *289–290*, 149. [CrossRef]
4. Brook, D.J.R. Coordination Chemistry of Verdazyl Radicals. *Comm. Inorg. Chem.* **2015**, *35*, 1–17. [CrossRef]
5. Miller, J.S. Magnetically ordered molecule-based materials. *Chem. Soc. Rev.* **2011**, *40*, 3266–3296. [CrossRef]
6. Luneau, D.; Rey, P. Magnetism of metal-nitroxide compounds involving bis-chelating imidazole and benzimidazole substituted nitronyl nitroxide free radicals. *Coord. Chem. Rev.* **2005**, *249*, 2591–2611. [CrossRef]
7. Caneschi, A.; Gatteschi, D.; Lalioti, N.; Sangregorio, C.; Sessoli, R.; Venturi, G.; Vindigni, A.; Rettori, A.; Pini, M.G.; Novak, M.A. Cobalt(II)-Nitronyl Nitroxide Chains as Molecular Magnetic Nanowires. *Angew. Chem. Int. Ed.* **2001**, *40*, 1760–1763. [CrossRef]
8. Liu, X.; Feng, X.; Meihaus, K.R.; Meng, X.; Zhang, Y.; Li, L.; Liu, J.-L.; Pedersen, K.S.; Keller, L.; Shi, W.; et al. Coercive Fields Above 6 T in Two Cobalt(II)–Radical Chain Compounds. *Angew. Chem.* **2020**, *132*, 10697–10705. [CrossRef]
9. Vaz, M.G.F.; Cassaro, R.A.A.; Akpinar, H.; Schlueter, J.A.; Lahti, P.M.; Novak, M. A Cobalt Pyrenylnitronylnitroxide Single-Chain Magnet with High Coercivity and Record Blocking Temperature. *Chem.-Eur. J.* **2014**, *20*, 5460–5467. [CrossRef]
10. Rancurel, C.; Leznoff, D.B.; Sutter, J.-P.; Golhen, S.; Ouahab, L.; Kliava, J.; Kahn, O. Synthesis, structure, and magnetism of mono- and binuclear manganese(II) compounds of nitronyl nitroxide substituted phosphine oxides. *Inorg. Chem.* **1999**, *38*, 4753–4758. [CrossRef]
11. Luneau, D.; Risoan, G.; Rey, P.; Grand, A.; Caneschi, A.; Gatteschi, D.; Laugier, J. Transition metal derivatives of a chelating nitronyl nitroxide ligand. Nickel(II) and manganese(II) complexes. *Inorg. Chem.* **1993**, *32*, 5616–5622. [CrossRef]
12. Tretyakov, E.V.; Koreneva, O.V.; Romanenko, G.V.; Shvedenkov, Y.G.; Ovcharenko, V.I. Synthesis, structure and magnetism of $M(hfac)_2$ complexes with spin labelled amides. *Polyhedron* **2004**, *23*, 763–772. [CrossRef]
13. Yu, Y.-X.; Hu, H.-M.; Zhang, D.-Q.; Wang, Z.-Y.; Zhu, D.-B. Two New Nitronyl Nitroxide Radicals and Their Complexes with $M(hfac)_2$ [M=Co(II), Ni(II), Mn(II)]: Syntheses, Crystal Structures, and Magnetic Characterizations. *Chin. J. Chem.* **2007**, *25*, 1259–1266. [CrossRef]
14. Zhang, C.-X.; Zhang, Y.-Y.; Zhang, H.-L.; Zhao, Y.; Sun, Y.-Q. Synthesis, structures and magnetic properties of nickel(II), manganic(II) and zinc(II) complexes containing pyridyl-substituted nitronyl nitroxide and tris(2-benzimidazolymethyl)amine. *Inorg. Chim. Acta* **2009**, *362*, 5231–5236. [CrossRef]
15. Zhang, Y.-J.; Wang, J.-J.; Huang, Q.; Chen, J. Crystal structures and magnetic properties of nitronyl nitroxide NIT2-phtrz and its M(II) hexafluoroacetylacetonate (M = manganese, copper) complexes $[M(hfac)_2(NIT2\text{-}phtrz)]$. *Transit. Met. Chem.* **2012**, *37*, 743–749. [CrossRef]
16. Li, T.; Shi, X.J.; Chen, P.Y.; Yu, S.J.; Tian, L. A series bi-spin transition metal(II) complexes based on triazole nitronyl nitroxide radical. *Inorg. Chim. Acta* **2017**, *461*, 206–212. [CrossRef]
17. Caneschi, A.; Gatteschi, D.; Sessoli, R.; Rey, P. Structure and magnetic properties of a ring of four spins formed by manganese(II) and a pyridine substituted nitronyl nitroxide. *Inorg. Chim. Acta* **1991**, *184*, 67–71. [CrossRef]
18. Wang, H.; Liu, Z.; Liu, C.; Zhang, D.; Lü, Z.; Geng, H.; Shuai, Z.; Zhu, D. Coordination Complexes of 2-(4-Quinolyl)nitronyl Nitroxide with $M(hfac)_2$ [M = Mn(II), Co(II), and Cu(II)]: Syntheses, Crystal Structures, and Magnetic Characterization. *Inorg. Chem.* **2004**, *43*, 4091–4098. [CrossRef]
19. Zhang, J.-Y.; Liu, C.-M.; Zhang, D.-Q.; Gao, S.; Zhu, D.-B. Syntheses, crystal structures, and magnetic properties of two cyclic dimer M_2L_2 complexes constructed from a new nitronyl nitroxide ligand and $M(hfac)_2$ ($M = Cu^{2+}$, Mn^{2+}). *Inorg. Chim. Acta* **2007**, *360*, 3553–3559. [CrossRef]
20. Liu, R.-N.; Li, L.-C.; Xing, X.-Y.; Liao, D.-Z. Cyclic metal–radical complexes based on 2-[4-(1-imidazole)phenyl]-4,4,5,5-tetramethylimidazoline-1-oxyl-3-oxide: Syntheses, crystal structures and magnetic properties. *Inorg. Chim. Acta* **2009**, *362*, 2253–2258. [CrossRef]
21. Wang, C.; Ma, Y.; Wang, Y.; Wang, Q.; Li, L.; Cheng, P.; Liao, D. A New Quinoxalinyl-Substituted Nitronyl Nitroxide Radical and its Five-Spin Cu^{II} and Four-Spin Mn^{II} Complexes: Syntheses, Crystal Structures, and Magnetic Properties. *Aust. J. Chem.* **2012**, *65*, 672–679. [CrossRef]
22. Tian, H.; Li, Y.; Zhang, C.; Mei, X.; Hu, P.; Li, L. Two novel cyclic dimer M_2L_2 complexes constructed from 2-[(4-carboxyl)phenyl]-4,4,5,5-tetramethylimidazoline-1-oxyl-3 oxide: Crystal structure and magnetic properties. *Polyhedron* **2013**, *52*, 1053–1058. [CrossRef]
23. Guo, J.-N.; Wang, J.-J.; Sun, G.-F.; Li, H.-D.; Li, L.-C. A novel nitronyl nitroxide radical containing thiophene and pyridine rings and its manganese(II) complex: Synthesis, structure, and magnetic properties. *J. Coord. Chem.* **2017**, *70*, 1926–1935. [CrossRef]

24. Zhu, M.; Lou, D.; Deng, X.; Zhang, L.; Zhang, W.; Lü, Y. A functional nitroxide ligand builds up two 2p–3d complexes with different spin ground states and a 2p–3d–4f chain of rings. *CrystEngComm* **2018**, *20*, 2583–2592. [CrossRef]
25. Yang, M.; Xie, S.; Liang, X.; Zhang, Y.; Dong, W. A novel functional nitronyl nitroxide and its manganese and cobalt complexes: Synthesis, structures and magnetic properties. *Polyhedron* **2019**, *161*, 132–136. [CrossRef]
26. Lin, H.-H.; Mohanta, S.; Lee, C.-J.; Wei, H.-H. Syntheses, Crystal Engineering, and Magnetic Property of a Dicyanamide Bridged Three-Dimensional Manganese(II)−Nitronyl Nitroxide Coordination Polymer Derived from a New Radical. *Inorg. Chem.* **2003**, *42*, 1584–1589. [CrossRef] [PubMed]
27. Gao, Y.-L.; Tian, C.; Gao, P.; Jiao, Y.; Gong, Y.; Ma, X. Synthesis, crystal structures, and magnetic properties of nitroxide radical-coordinated manganese(II) and cobalt(II) complexes. *J. Chem. Res.* **2021**, *45*, 788–794. [CrossRef]
28. Fegy, K.; Luneau, D.; Ohm, T.; Paulsen, C.; Rey, P. Two-Dimensional Nitroxide-Based Molecular Magnetic Materials. *Angew. Chem. Int. Ed.* **1998**, *37*, 1270–1273. [CrossRef]
29. Luneau, D.; Borta, A.; Chumakov, Y.; Jacquot, J.-F.; Jeanneau, E.; Lescop, C.; Rey, P. Molecular magnets based on two-dimensional Mn(II)–nitronyl nitroxide frameworks in layered structures. *Inorg. Chim. Acta* **2008**, *361*, 3669–3676. [CrossRef]
30. Lecourt, C.; Izumi, Y.; Khrouz, L.; Toche, F.; Chiriac, R.; Bélanger-Desmarais, N.; Reber, C.; Fabelo, O.; Inoue, K.; Desroches, C.; et al. Thermally-induced hysteretic valence tautomeric conversions in the solid state via two-step labile electron transfers in manganese-nitronyl nitroxide 2D-frameworks. *Dalton Trans.* **2020**, *49*, 15646–15662. [CrossRef]
31. Spinu, C.A.; Pichon, C.; Ionita, G.; Mocanu, T.; Calancea, S.; Raduca, M.; Sutter, J.-P.; Hillebrand, M.; Andruh, M. Synthesis, crystal structure, magnetic, spectroscopic, and theoretical investigations of two new nitronyl-nitroxide complexes. *J. Coord. Chem.* **2021**, *74*, 279–293. [CrossRef]
32. Stoll, S.; Schweiger, A. EasySpin, a comprehensive software package for spectral simulation and analysis in EPR. *J. Magn. Reson.* **2006**, *178*, 42–55. [CrossRef]
33. Kahn, O. *Molecular Magnetism*, 2nd ed.; Dover Publications: New York, NY, USA, 2021.
34. Sheldrick, G.M. Crystal structure refinement with SHELXL. *Acta Cryst.* **2015**, *C71*, 3–8.
35. Sheldrick, G.M. SHELXT—Integrated space-group and crystal structure determination. *Acta Cryst.* **2015**, *A71*, 3–8. [CrossRef]
36. Lever, A.B.P. *Inorganic Electronic Spectroscopy*, 2nd ed.; Elsevier: Amsterdam, The Netherlands, 1984; pp. 479–489.
37. Chilton, N.F.; Anderson, R.P.; Turner, L.D.; Soncini, A.; Murray, K.S. PHI: A powerful new program for the analysis of anisotropic monomeric and exchange-coupled polynuclear d- and f-block complexes. *J. Comput. Chem* **2013**, *34*, 1164–1175. [CrossRef]
38. Frisch, M.J.; Trucks, G.W.; Schlegel, H.B.; Scuseria, G.E.; Robb, M.A.; Cheeseman, J.R.; Scalmani, G.; Barone, V.; Mennucci, B.; Petersson, G.A.; et al. *GAUSSIAN 09*; Revision, C.01; Gaussian, Inc.: Wallingford, CT, USA, 2009.
39. Becke, A.D. Density-functional thermochemistry. III. The role of exact exchange. *J. Chem. Phys.* **1993**, *98*, 5648–5652. [CrossRef]
40. Valero, R.; Costa, R.; Moreira, I.d.P.R.; Truhlar, D.G.; Illas, F. Performance of the M06 family of exchange-correlation functionals for predicting magnetic coupling in organic and inorganic molecules. *J. Chem. Phys.* **2008**, *128*, 114103. [CrossRef]
41. Weigend, F.; Ahlrichs, R. Balanced basis sets of split valence, triple zeta valence and quadruple zeta valence quality for H to Rn: Design and assessment of accuracy. *Phys. Chem. Chem. Phys.* **2005**, *7*, 3297–3305. [CrossRef]
42. Ruiz, E.; Cano, J.; Alvarez, S.; Alemany, P. Broken symmetry approach to calculation of exchange coupling constants for homobinuclear and heterobinuclear transition metal complexes. *J. Comput. Chem.* **1999**, *20*, 1391–1400. [CrossRef]
43. Nishino, M.; Yamanaka, S.; Yoshioka, Y.; Yamaguchi, K. Theoretical Approaches to Direct Exchange Couplings between Divalent Chromium Ions in Naked Dimers, Tetramers, and Clusters. *J. Phys. Chem. A* **1997**, *101*, 705–712. [CrossRef]
44. Palii, A.V.; Korchagin, D.V.; Yureva, E.A.; Akimov, A.V.; Misochko, E.Y.; Shilov, G.V.; Talantsev, A.D.; Morgunov, R.B.; Aldoshin, S.M.; Tsukerblat, B.S. Single-Ion Magnet $Et_4N[Co^{II}(hfac)_3]$ with Nonuniaxial Anisotropy: Synthesis, Experimental Characterization, and Theoretical Modeling. *Inorg. Chem.* **2016**, *55*, 9696–9706. [CrossRef] [PubMed]
45. Lloret, F.; Julve, M.; Cano, J.; Ruiz-García, R.; Pardo, E. Magnetic properties of six-coordinated high-spin cobalt(II) complexes: Theoretical background and its application. *Inorg. Chim. Acta* **2008**, *361*, 3432–3445. [CrossRef]
46. Abragam, A.; Bleaney, B. *Electron Paramagnetic Resonance of Transition Metal Ions*; Clarendon Press: Oxford, UK, 1970; pp. 209–211.
47. Telser, J. EPR Interactions—Zero-field Splittings. In *eMagRes*; John Wiley & Sons, Ltd.: Chichester, UK, 2017; Volume 6, pp. 207–234.